Accuracy Improved Chua-type Vector Hysteresis Model and its Application to Iron Loss Analysis of Three-phase Induction Motor

Heesung Yoon, Minho Song, Pan Seok Shin*, and Chang Seop Koh, *Senior Member, IEEE*
College of ECE, Chungbuk National University, 410 sungbong-ro, Cheongju, Chungbuk 361-763, KOREA
*Dept. of EE, Hongik University, Jochiwon, Chungnam 339-701, KOREA
hsyoon@chungbuk.ac.kr

Abstract — This paper deals with an improved Chua-type vector hysteresis model and its implementation to the finite element method (FEM). The proposed model improves the modeling accuracy compared with the conventional one under the distorted magnetic flux condition. The proposed model combined with FEM is applied to iron loss estimation of a three-phase induction motor, and its validity is investigated through the comparison of the numerical result with the experimental one.

I. INTRODUCTION

It is well known that, in electrical machines, a considerable part of iron loss is caused by the rotating magnetic field [1]. For reducing the iron loss, therefore, a precise hysteresis model is required to predict not only alternating but also rotating magnetic properties accurately.

In order to describe the vector magnetic property for alternating and rotating magnetic fields, E&S model has been developed and applied to various applications such as three-phase transformer and induction motor [2]-[4]. Although this method precisely models the behavior of the magnetic field intensity for sinusoidal *B*-waveforms, it does not for saturated and distorted *B*-waveforms.

For the application to an electrical machine where the local parts are magnetically saturated and *B*-waveforms are distorted, the accuracy of the model should be improved.

In this paper, an improved Chua-type vector hysteresis model based on E&S model is proposed to increase the modeling accuracy under the distorted magnetic flux density condition. The developed model is combined with the finite element method (FEM) and applied to an iron loss analysis of a three-phase induction motor. Through a comparison with experimental result, the validity of the proposed algorithm is verified.

II. IMPROVED VECTOR HYSTERESIS MODEL

A. Chua-type Vector Hysteresis Model

In Chua-type vector hysteresis model which takes account of the classical eddy current field, the relationship between *B* and *H* is defined as follows [5]:

$$H_k(\tau)=\nu_k^r B_k(\tau)+\nu_k^i \frac{\partial B_k(\tau)}{\partial \tau}+\frac{\sigma\omega d^2}{12}\frac{\partial B_k(\tau)}{\partial \tau} \tag{1}$$

where the subscript k, hereinafter, will be referred to the rolling (R) and transverse (T) directions, respectively, ν^r and ν^i are magnetic reluctivity and hysteresis coefficient matrices, respectively. The magnetic reluctivity and hysteresis coefficients in (1) are defined as [5]:

$$\begin{aligned}\nu_k^r &= \left(f_{kc}\cdot R_{B_k}+f_{ks}\cdot I_{B_k}\right)\Big/\left(R_{B_k}^2+I_{B_k}^2\right)\\ \nu_k^i &= \left(f_{kc}\cdot I_{B_k}-f_{ks}\cdot R_{B_k}\right)\Big/\left(R_{B_k}^2+I_{B_k}^2\right)\end{aligned} \tag{2}$$

$$\begin{aligned}f_{kc}&=\sum_{n=1}^{N}\left\{R_{(2n-1)H_k}\sum_{k=1}^{n}{}_{(2n-1)}C_{(2k-1)}\sum_{i=0}^{n-k}{}_{(n-k)}C_i\cdot(-1)^{(2n-2k-i)}\cos^{(2n-2i-2)}\tau\right\}\\ f_{ks}&=\sum_{n=1}^{N}\left\{I_{(2n-1)H_k}\sum_{k=0}^{n-1}{}_{(2n-1)}C_{2k}\sum_{i=0}^{k}{}_{k}C_i\cdot(-1)^{(n-i-1)}\sin^{(2n-2i-2)}\tau\right\}\end{aligned} \tag{3}$$

The coefficients R_{B_k}, I_{B_k}, $R_{(2n-1)H_k}$ and $I_{(2n-1)H_k}$ in (2) and (3) are defined from the measured *B*- and *H*-waveforms under sinusoidal (elliptical) magnetic flux density condition for both alternating and rotating fields.

Since the reluctivity and hysteresis coefficient matrices in (2) are defined only for elliptical *B*-waveforms, a distorted *B*-waveform (B_R, B_T), to get corresponding coefficient matrices, should be approximated to a proper elliptical *B*-waveform (b_R, b_T), as follows:

$$\begin{aligned}b_R(\tau)&=B_{\max}\cos\varphi\cos\tau-\alpha B_{\max}\sin\varphi\sin\tau\\ b_T(\tau)&=B_{\max}\sin\varphi\cos\tau+\alpha B_{\max}\cos\varphi\sin\tau\end{aligned} \tag{4}$$

where α is defined as $B_{\min}/B_{\max}$ with the definition of $B_{\max}$, $B_{\min}$, φ the maximum and minimum magnitudes and inclination angle of the elliptical *B*-waveform.

B. Conventional Chua-type Vector Hysteresis Model

In conventional Chua-type vector hysteresis model, a distorted *B*-waveform is approximated to an elliptical one using its fundamental component, *i.e.*, the parameters $B_{\max}$, φ and α in (4) are defined using the fundamental component of the distorted *B*-waveform [2]-[5]. The *H*-waveform is modeled as follows:

$$H_k(\tau)=\nu_k^r(\tau)b_k(\tau)+\nu_k^i(\tau)\frac{\partial b_k(\tau)}{\partial \tau}+\frac{\sigma\omega d^2}{12}\frac{\partial B_k(\tau)}{\partial \tau} \tag{5}$$

where the coefficient matrices are calculated with $B_{\max}$, φ, α and τ.

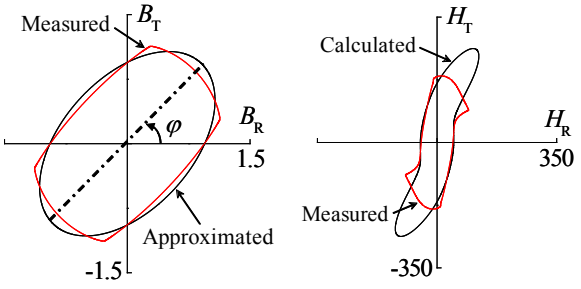

(a) *B*-waveform (b) *H*-waveform

Fig. 1. Conventional model under a distorted *B*-waveform for a non-oriented silicon steel sheet.

This method, for an elliptical *B*-waveform, is proven to present a reasonable *H*-waveform [2]-[5]. When applied to a distorted *B*-waveform, however, this method usually over-estimates B_{max} as shown in Fig. 1(a), and thus gives the *H*-waveform quite different from the measured one as shown in Fig 1(b).

C. Improved Chua-type Vector Hysteresis Model

In this model, a distorted *B*-waveform is approximated to an elliptical one, as shown in Fig. 2, by finding the parameters in (4) as follows:

- B_{max}: maximum magnitude of the distorted *B*-waveform
- φ: direction of the magnetic flux density at B_{max}
- α: numerically determined by minimizing the least square error between the distorted and approximated elliptical *B*-waveforms.

The *H*-waveform corresponding to the distorted *B*-waveform in this model is modeled as follows:

$$H_k(\tau)=\nu_k^r(\tau^*)B_k(\tau)+\nu_k^i(\tau^*)\frac{\partial b_k(\tau)}{\partial\tau}+\frac{\sigma\omega d^2}{12}\frac{\partial B_k(\tau)}{\partial\tau} \quad (6)$$

where the coefficient matrices are calculated with B_{max}, φ, α and τ*, and τ* defined in Fig. 2 is expressed as follows:

$$\tau^*=\cos^{-1}\left(\frac{\cos\varphi\, B_R(\tau)+\sin\varphi\, B_T(\tau)}{B_{max}}\right) \quad (7)$$

Fig. 3 compares the modeled *H*-waveform using the improved model with those from experimentally measured and the conventional model. It can be found that the modeling accuracy is a lot improved.

D. Implementation to FEM

In order to apply the proposed model to the finite element analysis, the governing equation is defined as follows:

$$\nabla\times\nu^r\nabla\times\mathbf{A}=\mathbf{J}_0-\nabla\times\left(\nu^i\frac{\partial\mathbf{b}}{\partial\tau}+\frac{\sigma\omega d^2}{12}\frac{\partial\mathbf{B}_{old}}{\partial\tau}\right) \quad (8)$$

where $\mathbf{B}_{old}$ is the *B*-waveform in the previous iteration, and $\mathbf{b}$ is defined as in (4) using $\mathbf{B}_{old}$. In the finite element formulation, equation (8) is approximated using Galerkin method together with circuit equations.

III. IRON LOSS ANALYSIS OF INDUCTION MOTOR

Fig. 4 shows the numerical results for a three-phase induction motor of which the rating power and voltage are 3.7kW and 380V, respectively. In order to compare the only pure iron loss without additional losses such as mechanical loss and friction loss, a rotor without slots and conducting bars is inserted and locked as shown in Fig. 4. In Fig. 4(a), it is observed that B_{max} in region A is almost same with that in region B. On the other hand, it is found that the iron loss in region A is bigger than that in region B as shown in Fig. 4(b). It is because that rotating magnetic fields are more concentrated in region A compared with region B and the rotational iron loss is generally larger than alternating one under same B_{max}.

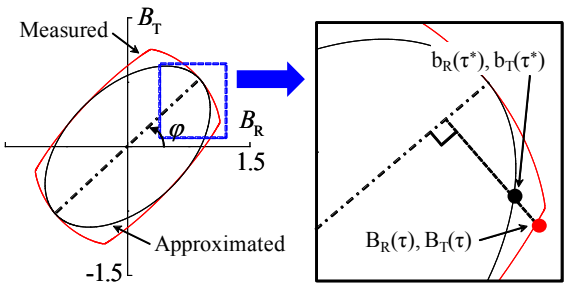

Fig. 2. Approximation of the distorted *B*-waveform to the elliptical one by using the proposed model.

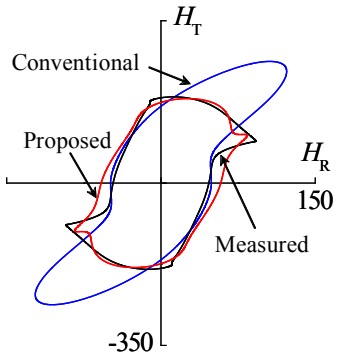

Fig. 3. Comparison of *H*-waveforms calculated by the proposed and conventional model with the experimental result.

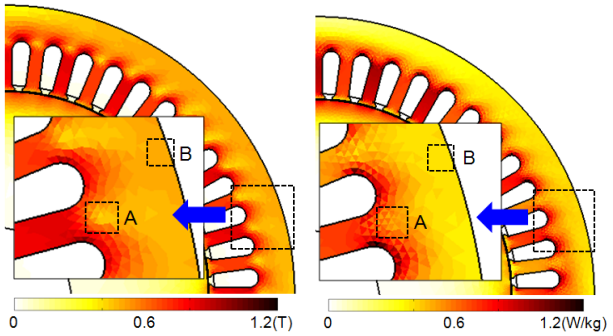

(a) B_{max} (b) iron loss

Fig. 4. Numerical results for iron loss analysis.

In the version of the full paper, the iron loss calculated by using the proposed method will be compared with the experimental result.

IV. REFERENCES

[1] A. J. Moses, "Importance of rotational losses in rotating machines and transformers," *Journal of Mat. Eng. and Perf.*, vol. 1, no. 2, pp. 235-244, 1992.

[2] M. Enokizono, and K. Okamato, "Designing a low-loss induction motor considering the vector magnetic properties," *IEEE Trans on. Magn.*, vol. 38, vol. 2, pp. 877-880, Mar., 2002.

[3] S. Urata, M. Enokizono, T. Todaka, and H. Shimoji, "The calculation considered two-dimensional vector magnetic properties depending on frequency of transformer," *IEEE Trans. on. Magn.*, vol. 42, no. 4, pp. 687-690, Apr. 2006.

[4] T. Sato, T. Todaka, and M. Enokizono, "Improvement of integral-type dynamic E&S modeling," *in Proceeding of CEFC 2010*, Chicago, USA, May 2010.

[5] M. Song, H. Yoon, P. S. Shin, and C. S. Koh, "A generalized Chua-type vector hysteresis model for both the non-oriented and grain-oriented electrical steel sheets," *in Proceeding of CEFC 2010*, Chicago, USA, May 2010.